ELSEVIER

Chemical Engineering Journal 75 (1999) 93–103

Chemical Engineering Journal

www.elsevier.com/locate/cej

The study of calcium oxalate precipitation using image analysis

B. Bernard-Michel[a], M.N. Pons[a,*], H. Vivier[a], S. Rohani[b]

[a]*Laboratoire des Sciences du Génie Chimique, CNRS-ENSIC-INPL 1, rue Grandville BP 451, 54 001 Nancy cedex, France*
[b]*Department of Chemical Engineering, University of Saskatchewan, Saskatoon, Canada*

Received 7 July 1998; received in revised form 3 March 1999; accepted 12 April 1999

Abstract

Image analysis is applied to study the precipitation of calcium oxalate in a semi-batch single- and double-feed reactor. The feed consists in un-premixed potassium oxalate and calcium chloride solutions. The effect of various operating conditions and feeding strategies on the yield of calcium oxalate mono-, di-, and tri-hydrates, the degree of agglomeration, and the crystal size is studied by image analysis. Statistical validity of the image analysis for crystal shape characterization and experimental precision is carefully investigated. Agglomeration and face growth kinetics are quantified.

Keywords: Calcium oxalate; Image analysis; Agglomeration

1. Introduction

Morphology is an important characteristic of crystallized and precipitated materials that affects product end-use properties. Operating conditions such as temperature, addition of habit modifiers, reactant concentrations, reactor design and control and feeding strategy, are known to affect particle morphology in precipitation and crystallization processes.

Depending upon the operating conditions calcium oxalate forms three hydrates: monohydrate (COM), dihydrate (COD) and trihydrate (COT). Calcium oxalate precipitation is therefore an interesting process to investigate. So Garside et al. [1] studied the effect of temperature on the precipitation of calcium oxalate in a MSMPR crystallizer. Brecevic et al. [2] investigated the effect of factors such as initial feed composition and type of stirring on the distribution of hydrate types in calcium oxalate precipitation in lab-scale experiments. This reaction was also selected by Houcine et al. [3] to study the effect of similar factors on a pilot-scale reactor. Basing their experimental evidence on calcium oxalate precipitation Marcant and David [4], and David and Marcant [5] developed methods for predicting the micromixing effects in single-jet and double-jet precipitators. Recently Bramley et al. [6] studied calcium oxalate aggregation, the second crystal enlargement process to growth.

Calcium oxalate is also receiving large interest from a medical point of view as urinary calculi contain calcium oxalate as one of the major components. Tomazic and Nancollas [7], and Lepage and Tawashi [8] studied the kinetics of dissolution of calcium oxalate hydrates in pure water or saline solutions mimicking urine. The development of the hydrates in presence of various substances of medical interest has been investigated: L-glutamic acid by DeLong and Briedis [9], polyhydroxycarboxylic acids by Grases et al. [10], mucin by Akbarich and Tawashi [11], dodecylammonium chloride by Skrtic et al. [12].

New techniques have also been proposed to study the growth of calcium oxalates hydrates using the uptake of ^{45}Ca [13] or a micro-crystallizer [9]. All these studies were based on classical tools (particle size analyzers, X-ray diffraction and thermogravimetric analysis) and the morphological changes are assessed qualitatively as it is done in most precipitation studies.

However, nowadays, image analysis offers a way to quantify the variations of crystal habit. Shape and size can be characterized subsequent to the visualization of the crystals by light or electron microscopy. The quantitative description of the morphology of a particle population is based on the use of different shape descriptors [14,15]. These techniques have previously being applied to some oxalate species [16–18]. The purpose of this contribution is to describe a methodology to have more insights in the precipitation of calcium oxalate, especially concerning the

*Corresponding author.

1385-8947/99/$ – see front matter
PII: S1385-8947(99)00077-7

agglomeration and growth kinetics, using the information provided by image analysis.

2. Materials and methods

2.1. Experimentals

Experiments were carried out in a 2 l stainless steel jacketed rounded-bottom reactor (Fig. 1) at a constant stirring rate of 500 rpm. A Rushton turbine, which produces a fast homogenization at the small scales of mixing [3] was used as stirring device. Temperature was controlled at 22°C by a water bath. The reactor contained initially deionized water (V_0=1.6 l). Equal volumes of potassium oxalate (V_K) and calcium chloride (V_{Ca}) solutions were added with $V_K=V_0/\alpha$ and α=100. The concentrations were calculated in order to have an overall supersaturation degree σ equal to 190, with σ defined by:

$$\sigma = \frac{[Ox^{2-}][Ca^{2+}]}{K_s} - 1, \quad (1)$$

where $[Ox^{2-}]$ and $[Ca^{2+}]$ are respectively the concentrations in oxalate and calcium ions. Due to the relatively low concentrations, activity coefficients were not considered here [19]. K_s is the solubility product whose value at 22°C was found in literature [20] to be equal to 2.162×10^{-9} mol^2 l^{-2}. Single and double jets experiments were conducted at several flow rates (Table 1). The oxalate and calcium concentrations in the feed solutions were 0.1 M.

At the end of each run, 1–2 cm^3 of the crystal suspension was filtered by carefully spreading the sample on a filtering membrane (cellulose nitrate, pore size=0.2 μm) with the help of a peristaltic pump. This was done in order to limit crystal overlapping. After filtration and drying, pieces of the membrane were fixed on a support and gold-plated for examination by a scanning electron microscope (T330A, Jeol, Rueil-Malmaison, France). About 80 crystals per sample were analyzed. Digital images on 256 grey levels were captured and transferred to a workstation on which the image analysis packages were implemented. Visilog 4.1.4^{TM} (Noesis, Les Ulis, France) in conjunction with a package developed in our laboratory were used for the analysis of the images.

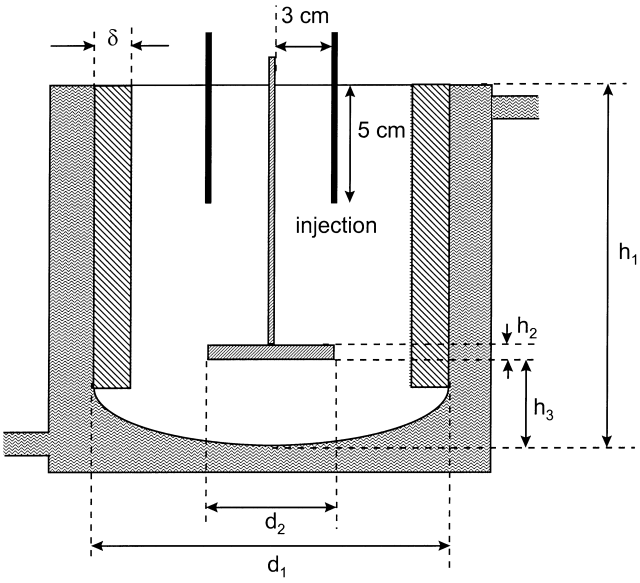

Fig. 1. Experimental set-up (h_1=0.16 m, h_2=0.006 m, h_3=0.042 m, d_1=0.14 m, d_2=0.046 m, δ=0.014 m).

Table 1
Experimental operating conditions (for the double feed strategy, both flowrates are equal)

Experiment	Feeding strategy	Flow rate (ml/h)
1	Double feed	10
2	Double feed	80
3	Double feed	300
4	Double feed	800
5	Double feed	Infinite
6	Single feed	10
7	Single feed	80
8	Single feed	300
8R (repetition of exp8)	Single feed	300
9	Single feed	800
10	Single feed	Infinite

The concentration of ions in solution during crystallization was obtained from measurements of electrical conductance by means of a calibrated conductance cell (Radiometer, Copenhagen, Denmark), connected to a CD810 conductimeter (Tacussel, Villeurbanne, France). The relationship between conductivity and concentrations was expressed using standard equivalent conductances.

2.2. Image analysis

Fig. 2 presents four images illustrating the main stages of the treatment. Treatment of image A, by contour enhancement, thresholding and filling of the contour, produces image B which contains the particle silhouette. Due to the presence of filter, manual editing, using the graphical capabilities of Visilog^{TM}, is generally necessary. Image C contains the particle silhouette polygonal hull (H_c), i.e. the smallest analog convex polygon in which the particle is inscribed and image D contains the crystal facets.

Primary parameters are computed on the particle silhouette (image B): surface S, from which the surface-equivalent-diameter $D_{eq} = 2\sqrt{S/\pi}$ is deduced, perimeter P, Feret diameter distribution, from which the maximal diameter (F_{max}) (i.e. silhouette "length") and minimal diameter (F_{min}) (i.e. silhouette "width") are extracted. Dimensionless secondary parameters (circularity, $C=P^2/(4\pi S)$, ratios F_{max}/F_{min} and F_{max}/D_{eq}) are calculated.

The particle silhouette is compared to its convex hull H_c (image C). Let ω_1 and ω_2 be, respectively the number of erosions necessary to eliminate completely the particle

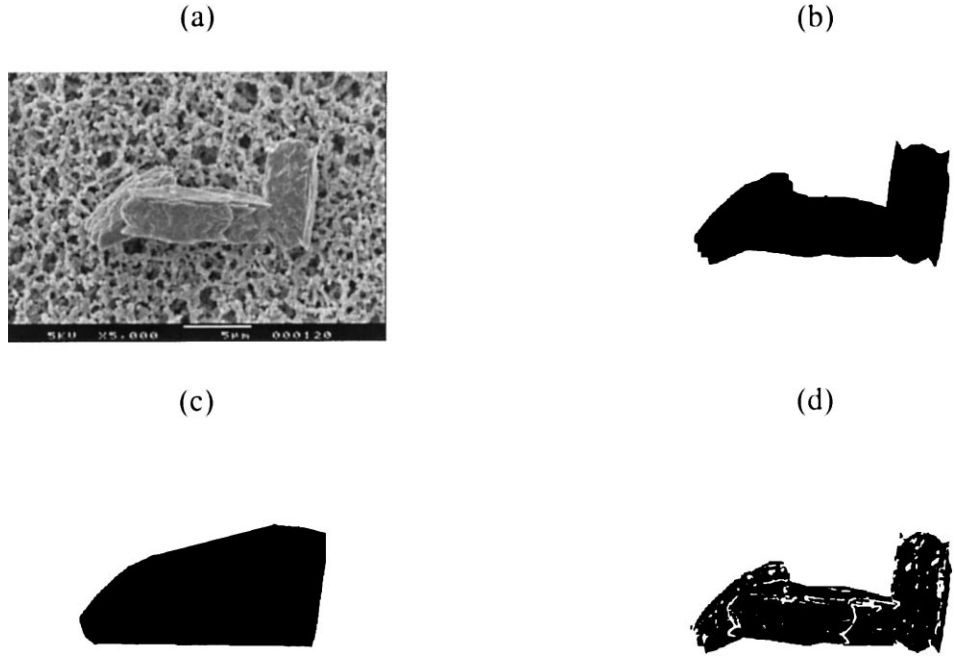

Fig. 2. Grey level image A (a), particle silhouette B (b), convex hull silhouette C (c); particle facets (d).

silhouette and its complement with respect to H_c (of surface S_c). Following the concepts of mathematical morphology in a discrete space of square grid [21], this means that the particle silhouette has a size equivalent to $(2\omega_2+1)^2$ pixels and the largest concavity (i.e. the last one to disappear in the erosion process) a size equivalent to $(2\omega_2+1)^2$. The magnification chosen for the imaging being such that $2\omega_1 \gg 1$ and $2\omega_2 \gg 1$, two dimensionless shape descriptors are computed: $\Omega_1 = 2\omega_1/\sqrt{S}$ which characterizes the particle robustness and $\Omega_2 = 2\omega_2/\sqrt{S}$ which describes the largest concavity [22]. A surface concavity index, $CI=S/S_c$, which quantifies globally the concavity of the object, is computed.

A parameter representing the complexity of the network of facets of the crystals is computed by determining the partition-in-squares: it is based on the distribution of squares inscribed in an object (in the case of the particle silhouette) or a set of objects (in the case of the particle facets) (image D). The principle is to divide the zones between edges (borderline, facet edges) into squares of increasing size, so that the total available area is covered. This results in a distribution in number $f(u)$ of squares of normalized side length, $u = x/\sqrt{S}$, where x is the side length of the square. A simplicity index ξ is defined from $f_{facet}(u)$ and $f_{silhouette}(u)$ which are respectively the distributions calculated for the particle facets and for its silhouette [23]. ξ is equal to 1 for a particle without any facet.

2.3. Statistics

The selection of a representative sample and the experimental precision require special attention in the study of a crystallization process by image analysis. Different statistical tests have been used.

When only average values are of interest, the comparison of two samples (from the same population or from two different populations) is based on the parametric test on average values ($\bar{x}$ test). If, on another hand, distribution representativity is needed, two additional tests are necessary, the parametric test on standard deviations (s test) and the non parametric U-test of Mann and Whitney [24].

Depending upon the selected test, the null hypothesis H_0 is expressed as ''means, standard deviations or distributions are equal''. The error probability α characterizes the risk of taking the wrong decision when concluding that H_0 is false. Critical values are defined: $\alpha_c=5\%$ (rejection criterion), $\alpha_{c_1}=1\%$ and $\alpha_{c_2}=0.05\%$.

- $\alpha>\alpha_c$: the tested values are equal.
- $\alpha_c>\alpha>\alpha_{c_1}$: they are marginaly significatively different.
- $\alpha_{c_1}>\alpha>\alpha_{c_2}$: they are significatively different.
- $\alpha_{c_2}>\alpha$: they are very significatively different.

With a careful preparation of the samples 80 crystals were sufficient to statistically represent a population. Similar results have been obtained for copper sulphate crystals [25].

In order to check repeatability of the experiments, experiment 8 was replicated (experiment 8R in Table 2). Both runs were performed on the same day using the same aqueous solutions. The statistical tests (Table 2) were satisfactory on the average values ($\alpha>\alpha_c$) but not on the distributions (s and U tests). s test is the most difficult to satisfy. Despite the extreme care which was exercised to replicate the experiments exactly, it exists slight differences in the supersaturation curves of experiments 8 and 8R as shown in Fig. 3.

Table 2
Statistical tests on the experiment 8 repetition (bold values indicate parameters for which $\alpha > \alpha_c$ is not verified)

	$\bar{x}$ test (%)	s test (%)	U test (%)
Diameter	15.2	31	**0.3**
C	70.2	**0.07**	8.3
F_{max}/F_{min}	39.3	**0.44**	7.3
F_{max}/D_{eq}	13.9	22.1	6.4
Ω_1	61.8	45.7	34
Ω_2	57	9.8	47
CI	81.2	**0.027**	14
ξ	49	**0.75**	46

3. Results

3.1. Global shape and size characterization

Image analysis can be used as a tool to characterize the size and shape of the final product and to relate them to the operating conditions. As seen in Section 2.2 several shape descriptors are necessary to describe the shape. A simple method to have a rapid insight into the variations of those descriptors consists of summarizing all the morphological informations using the principal component analysis (PCA) [26,27]. Generally the two first principal components (f_1 and f_2) are used and differences in crystal shapes can be easily spotted by different locations of their representative points in the f_1-f_2 plane. Two neighboring points in the plane correspond to two crystals with similar shapes. In the present study, 85% of the morphological information was summarized in the f_1-f_2 plane (Fig. 4). Experiments 3 (double feed at 300 ml/h) and 7 (single feed at 80 ml/h) produced crystals with similar size (about 9 μm), but different shapes. This example illustrates that this method is capable of characterizing crystals according to their shape and size.

3.2. Detailed shape and size characterization

The global shape and size characterization, discussed above, provides information which allows to classify crystals in different shape categories. In the case of calcium oxalate, five shape groups can be defined: monohydrates, which could present two stable positions from the mechanical point of view (monohydrates1 or monohydrates2), depending upon the face growth rates, dihydrates, trihydrates, and agglomerates (Fig. 5 and Table 3). Monohydrate1 and monohydrate2 have roughly the same shape, except than monohydrate1 can be considered to be thicker than monohydrate2, with a larger growth rate of face 2 (Fig. 9). In monohydrate1, differences can be furthermore noticed in the growth rate of face 1: compact crystals are generally obtained at high supersaturation.

To illustrate the use of such a classification the effect of the feeding strategy on the yield of calcium oxalate hydrates has been examined by calculating the yield of each hydrate

Table 3
Characteristic descriptor values for the different shapes

	F_{max}/F_{min}	F_{max}/D_{eq}	C	CI	Ω_2	Ω_1	ξ
Monohydrate1	2.30	1.53	1.84	0.095	0.095	0.57	0.33
Monohydrate2	2.64	1.6	1.45	0.006	0.033	0.54	0.59
Dihydrate	1.36	1.21	1.20	0.005	0.022	0.78	0.90
Trihydrate	2.94	1.71	1.83	0.078	0.085	0.53	0.72
Agglomerate	–	–	>2	>0.15	>0.1	–	–

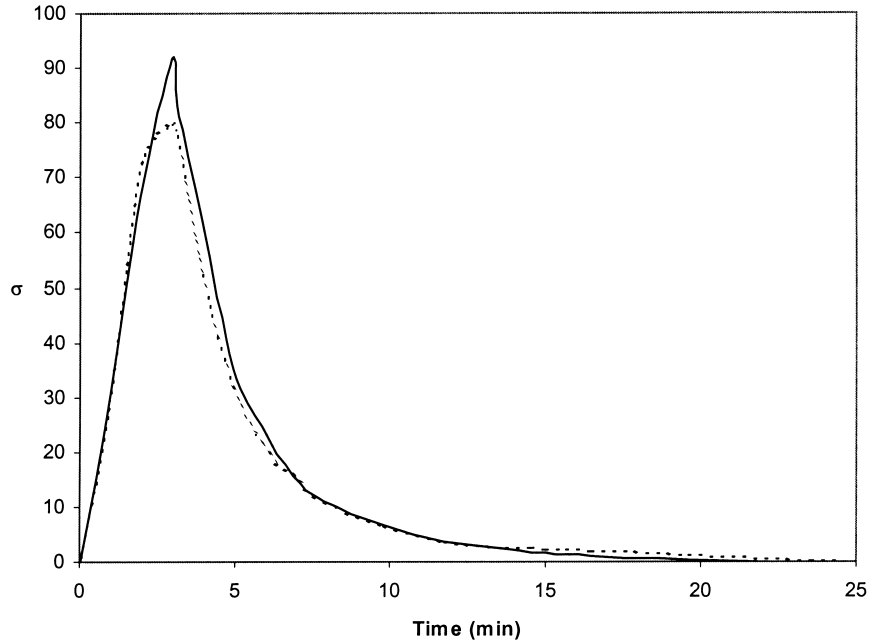

Fig. 3. Supersaturation curves for experiments 8 and 8R (——— exp8, - - - exp8R).

(a)

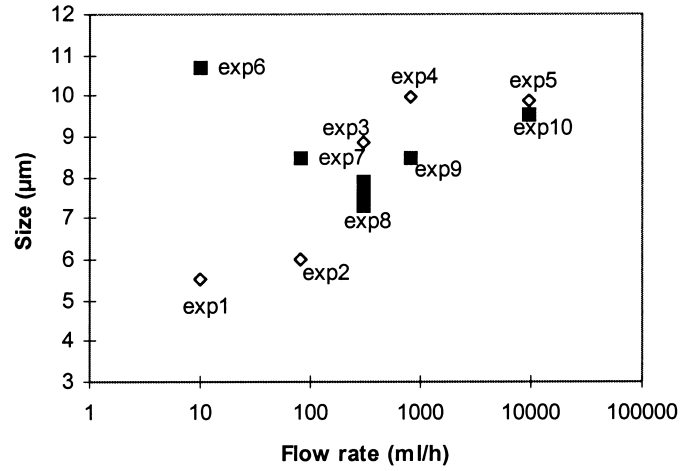

(b)

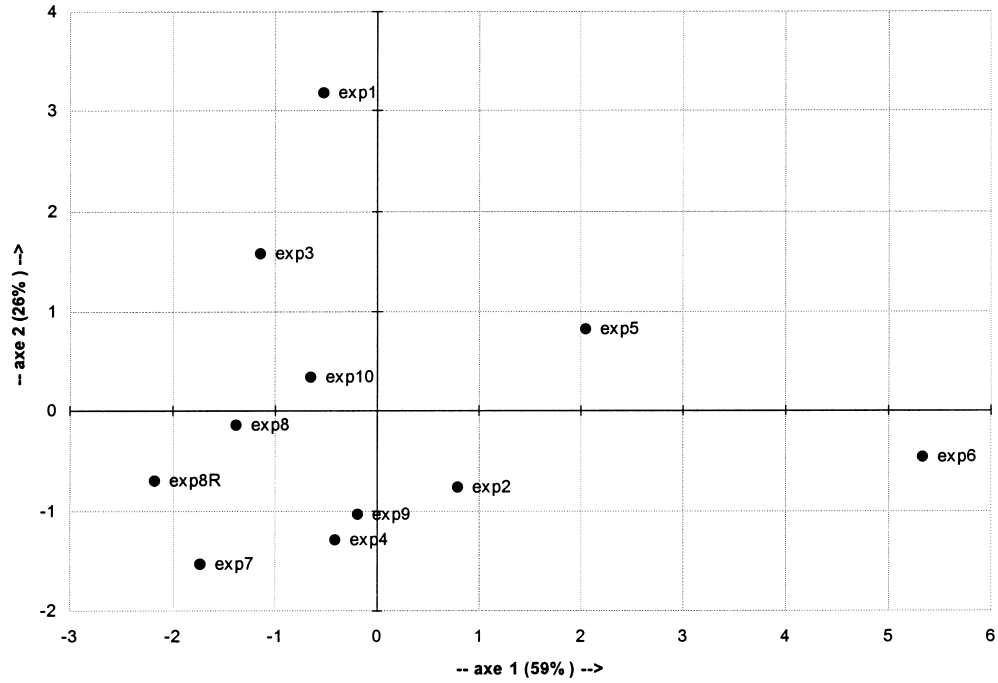

Fig. 4. (a) Average size results; ((◇) double feed strategy, (■) single feed strategy). The points at 10 000 ml/h represent the cases of infinite flowrate. (b) PCA morphological results.

among the total single crystal population. Precision is about 10%. Monohydrate crystals are the stable form and are predominant in all the experiments (Fig. 6), with a slightly larger yield in the single feed experiments. The dihydrates are very few and almost negligible. For the double feed strategy, the evolution of the trihydrates is quite irregular, while for single feed strategy, trihydrates appear only at infinite flow rate. These results are similar to those obtained by Marcant and David [4], and David and Marcant [5]: they precipitated only monohydrates in single feed experiments and mostly COM with some dihydrates and trihydrates in double-feed experiments.

Agglomeration is an important and complex phenomenon which occurs in most of crystallization processes. It is often neglected in the population balance to simplify calculations. Quantifying agglomeration using image analysis can help understanding this phenomenon and may lead to reasonable agglomeration models. As seen in Table 3 the agglomerates can be easily distinguished by their high values of circularity, concavity index and Ω_2. The crystals are here simply

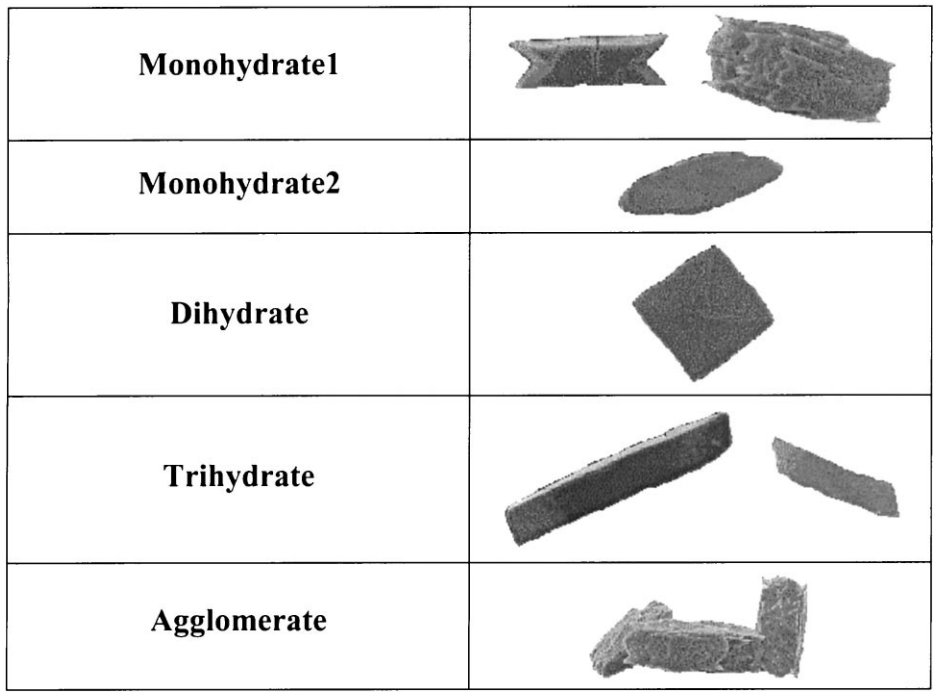

Fig. 5. The five morphological groups.

classified in two groups, single crystals and agglomerates. The mean size of a crystal population (L) can be defined in terms of the mean size of the single crystals (L_{mon}) and the agglomerates (L_{agg}) and their corresponding number fractions (X_{mon} and X_{agg} respectively):

$$L = X_{mon}L_{mon} + X_{agg}L_{agg}, \quad (2)$$

i.e.

$$L = L_{mon}\left(1 + X_{agg}\frac{L_{agg} - L_{mon}}{L_{mon}}\right) = L_{mon}(1 + \mathrm{INF}), \quad (3)$$

where INF is the agglomeration parameter.

If INF=0, agglomeration can be neglected. In order for INF to be zero either X_{agg} has to be zero or $(L_{agg}-L_{mon})/L_{mon}=0$. In the first case, all the crystals are single crystals and it is clear that agglomeration is negligible. In the second case, agglomeration is present, but agglomerates have the same size (growth rate) as single crystals. They can be considered as single crystals and agglomeration can be neglected in the population balance.

From that point of view very different results were obtained for the single-feed and double-feed experiments. In the case of the double-feed process, agglomerate sizes have the same evolution as monocrystals size (Fig. 7(c)).

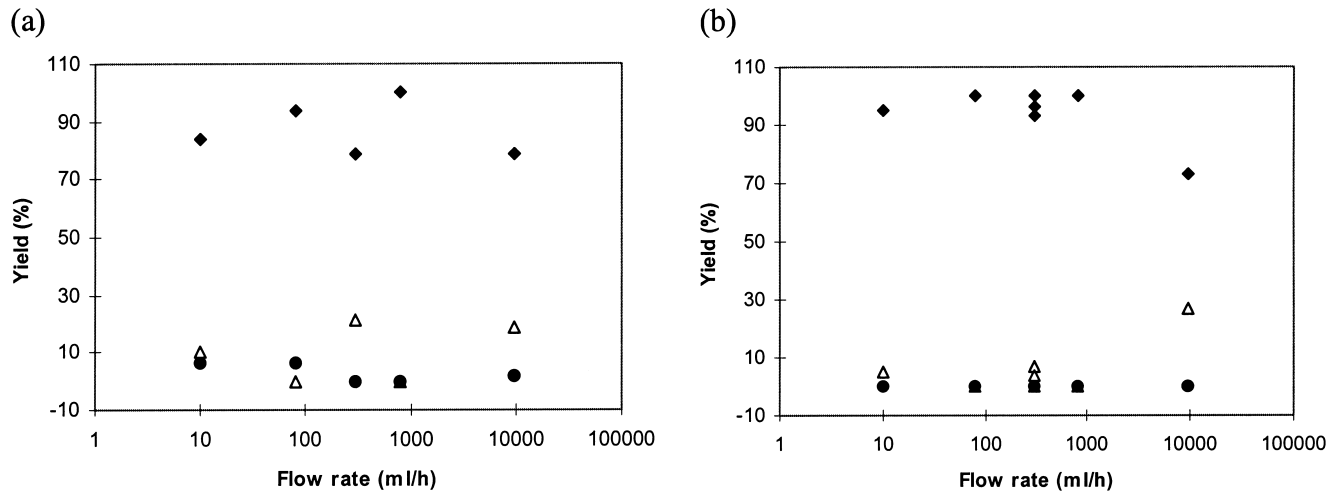

Fig. 6. Hydrates distribution; (a) double feed; (b) single feed; ((◆) monohydrates, (●) dihydrates, (△) trihydrates). The points at 10 000 ml/h represent the cases of infinite flowrate.

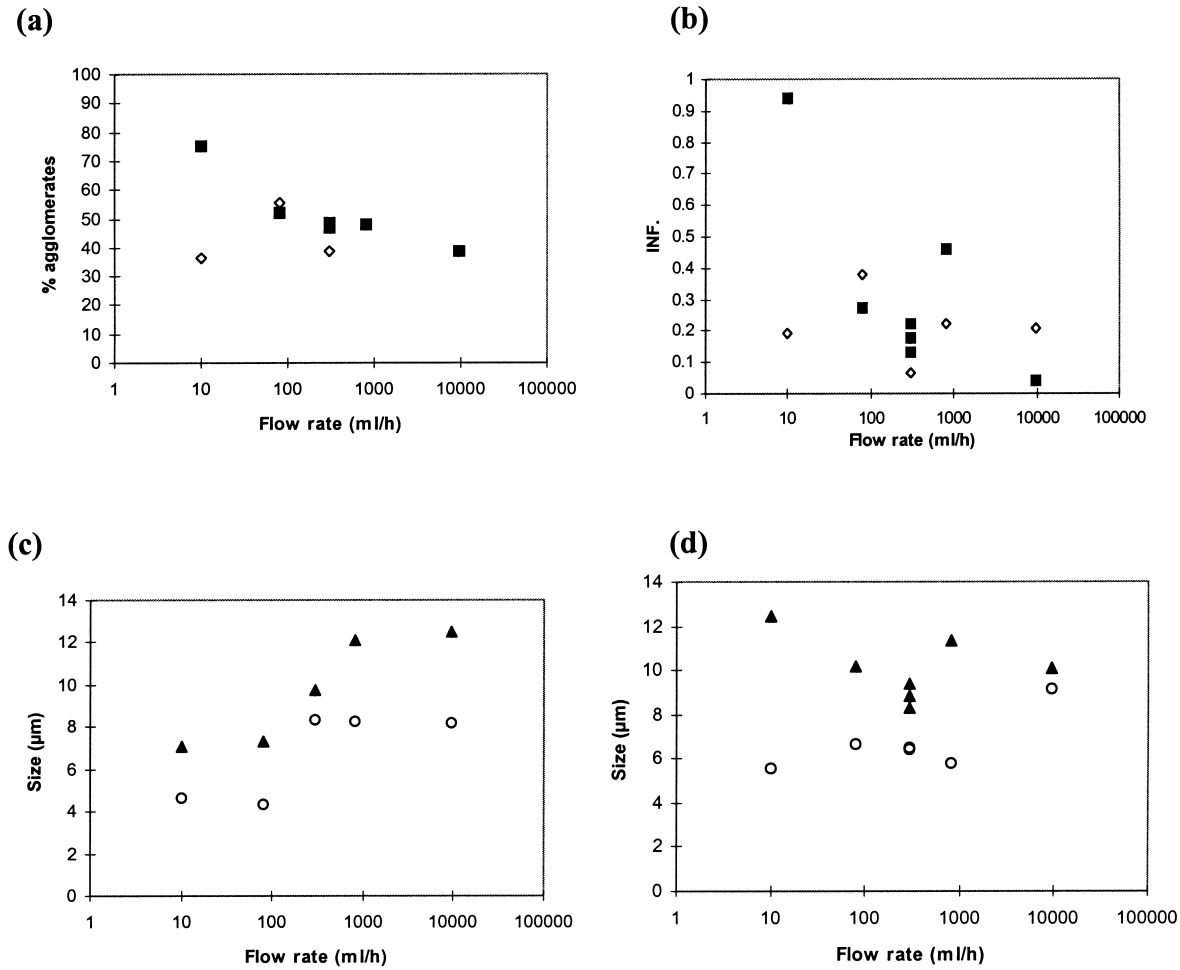

Fig. 7. Agglomeration study; (a) percentage of agglomerate ((◇) double feed, (■) single feed); (b) agglomeration influence ((◇) double feed, (■) single feed). Single crystals and agglomerates sizes (c) for double feed (d) for single feed ((○) single crystals, (▲) agglomerates). The points at 10 000 ml/h represent the cases of infinite flowrate.

For the single-feed process, size evolutions of single crystals and agglomerates are inversed (Fig. 7(d)). Influence of agglomeration on size is negligible for experiments 3 and 10 (Fig. 7(b)) whereas the percentage of agglomerates is about 40% (Fig. 7(a)). Visual examination revealed that the agglomerates seem to be mostly composed of two or three crystals. For these experiments, it is possible to neglect agglomeration in the population balance, but it is important

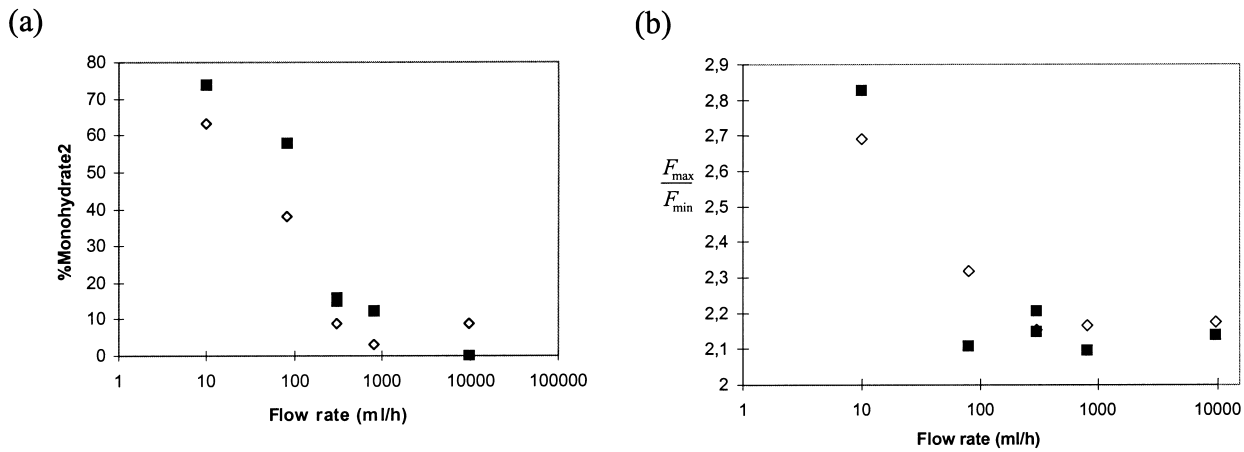

Fig. 8. (a) Percentage of Monohydrate2 compared to total monohydrates, (b) evolution of elongation (F_{max}/F_{min}) of monohydrate1 ((◇) double feed, (■) single feed). The points at 10 000 ml/h represent the cases of infinite flowrate.

to keep in mind that the shape of the product crystals is quite different from ideal monocrystals. In the other experiments, agglomeration has a more important effect, particularly in experiments 2, 6 and 9 where, in fact, the final size of the crystals is rather due to agglomeration than to pure growth.

Once the monohydrate crystals have been recognized and isolated, their directional growth can be quantified. The evolutions of the ratio of monohydrate2 compared to total monohydrates (Fig. 8(a)) and the F_{max}/F_{min} parameter evolution (Fig. 8(b)) for monohydrate1 show the importance of this phenomenon. High feedrates produce mostly compact monohydrate1.

3.3. Face growth kinetics

The cross-section of monohydrate monocrystals is approximatively inscribed in a rectangle: monohydrates can be characterized by the three dimensions L_1, L_2, L_3 (Fig. 9). L_2 and L_3 are directly given by the minimal Feret diameters, F_{min}(silhouette "width"). L_1 was calculated using $L_1=S/L_2$ (approximation of a rectangle). Once these parameters are determined, it is possible to estimate the directional growth using the classical growth theory for each face.

Table 4
Nucleation times t_i and times of maximum of the supersaturation curve (t_m)

Experiment	t_i (s)	t_m (s)
1	3745	2472
2	523	470
3	217	200
4	77	71
5	7.8	5.9
6	3840	1200
7	425	468
8	175	176
9	98	88
10	5.6	7.2

The interesting aspect of this approach is that the calculation of the kinetics is not based on distributions or average values. Only a targeted group of crystals are needed. Another important point is that the growth rate phenomenon is isolated. Agglomerates are not taken into account as nucleation does not have to be modeled and there is no need for the population balance. The last interesting point is that kinetics are determined for the three faces of crystals (directional growth).

$N=10$ experiments have been carried out in total. Supersaturation curves have been obtained from the conductivity measurements and the feedrates. Image analysis allows to separate monocrystals from the overall population. Each monocrystal is characterized by two of the three lengths L_1, L_2 and L_3, depending upon the growth rate of face 1. Assuming a different but constant growth rate for each crystal face it is possible to identify in each experiment i a group of monocrystals which have nucleated at the same

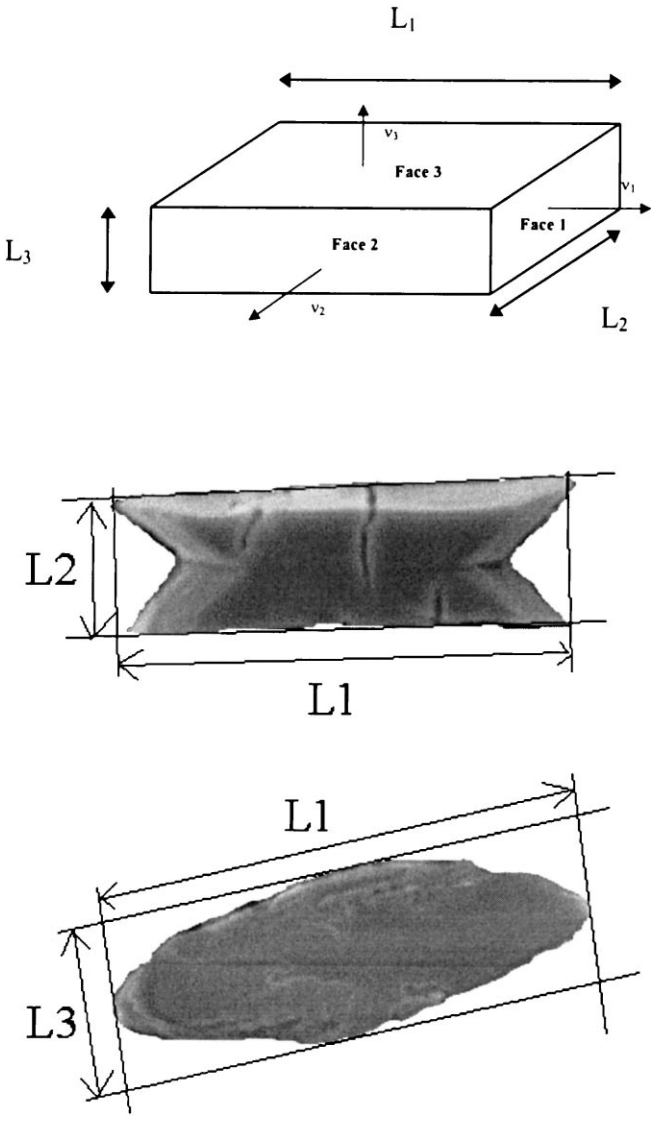

Fig. 9. The three characteristic lengths of monohydrate single crystals.

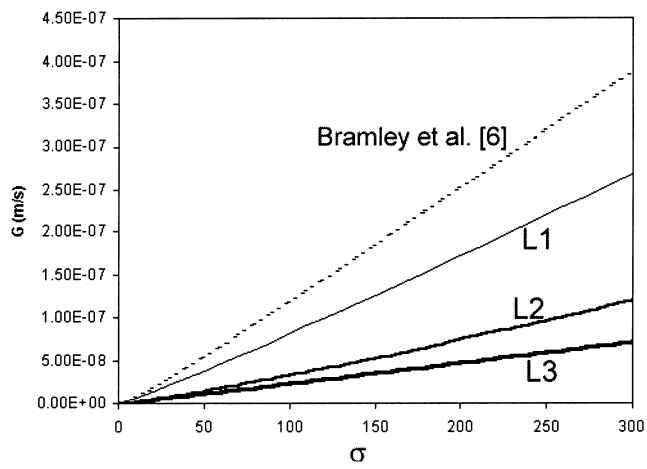

Fig. 10. Comparison of the face growth rates with literature data.

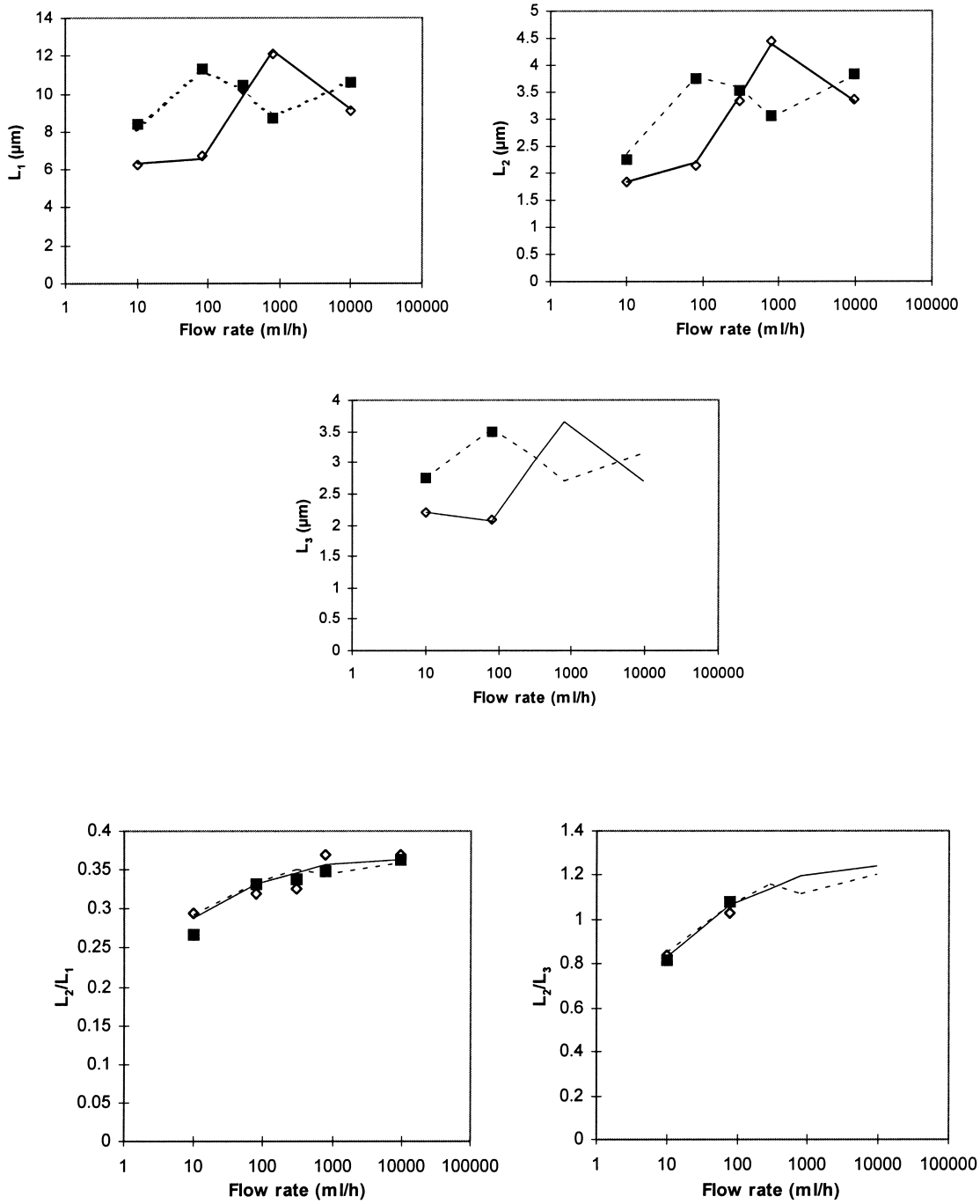

Fig. 11. Comparison between experimental and calculated size and shape characteristics ((◇) experiment double feed, (■) experiment single feed, (———) model double feed, (- - -) model single feed). The points at 10 000 ml/h represent the cases of infinite flowrate. Lines have been drawn for model results to facilitate the reading of the plots.

time t_i. Three growth rates can be estimated [28]:

$$G_j = k_j \sigma^{n_j} \ (j = 1 \text{ to } 3). \tag{4}$$

The final sizes of the group of crystals under consideration are

$$L_{i,j} = \int_{t_i}^{t_f} k_j \sigma(t)^{n_j} \mathrm{d}t \quad i = 1 \text{ to } N;\ j = 1 \text{ to } 3. \tag{5}$$

In our study, the group of crystals considered for each experiment i is the majority group (maximum of the population distribution from the point of view of L_1, L_2 and L_3).

The unknown parameters are t_i (i=1 to N), k_j and n_j (j=1 to 3). An optimization procedure, based on the box complex method [26] has been carried out by minimizing the objective function:

$$f_{\text{obj}} = \sum_{i=1,N} \sum_{j=1,3} \left(\frac{L_{i,j,\text{calc}} - L_{i,j,\text{exp}}}{L_{i,j,\text{exp}}} \right)^2. \tag{6}$$

Crystal shape constraints are added (ratios $r_{i,1}=L_{i,1}/L_{i,2}$ and $r_{i,2}=L_{i,1}/L_{i,3}$) to help the convergence and suppress eventual local minima. These constraints are expressed by:

$$\left|\frac{r_{i,m,\text{calc}} - r_{i,m,\text{exp}}}{r_{i,m,\text{exp}}}\right| m = 1,2 \ < 5\%. \quad (7)$$

For our experiments, the relative errors on the three face sizes were all less than 5%. The model fitting procedure determined nucleation times t_i close to the time when the maximum of the supersaturation curves (Table 4) occurred, except for very low feedrates. The following kinetic parameters were obtained:

$k_1=5.655\times10^{-4}$ μm/s, $n_1=1.08$;
$k_2=1.427\times10^{-4}$ μm/s, $n_2=1.18$;
$k_3=2.165\times10^{-4}$ μm/s, $n_3=1.02$.

The values found for n_j are consistent with the n value reported in the literature by Bramley et al. [6]. Fig. 10 compares the G_j values found in the present study with the results of Bramley et al. [6]. k_j values are lower than the value found by those authors because in their study, monocrystals were not isolated from the overall population. Therefore, agglomeration has exerted an influence on the size and the growth rate. The good agreement between our theoretical and experimental results are shown in Fig. 11 for the size (L_1, L_2, L_3) and shape characteristics.

4. Conclusion

Informations on the size, shape and growth characteristics of calcium oxalate hydrates have been obtained by semi-automated analysis of SEM images. This method also provides a mean to quantify complex processes such as agglomeration. The automation allows to base the data on a representative population of crystals. It might not be as large as the population examined by classical particle size analyzers such as laser diffraction granulometers, but these devices do not give information on the shape: they even demand it to produce reliable size distributions, when the particles are not spherical. There is indeed a compromise to accept between the time necessary for image capture (with SEM it is the limiting step) and the number of crystals. The technique can of course be applied to larger crystals, which can be easily observed by light microscopy.

With shape descriptors and methods to interpret the data, the background is now set for a more widespread use of image analysis to study precipitation and crystallization processes from the point of view of the understanding of the phenomena of nucleation, growth and agglomeration and of the improvement of the crystal end-use properties (effects of design and operation parameters, presence of additives and contaminants, etc).

5. Nomenclature

$C=P^2/(4\pi S)$	circularity
CI	concavity index
D_{eq}	surface-equivalent-diameter (m)
F_{max}	maximum Feret diameter (m)
F_{min}	minimum Feret diameter (m)
f_{obj}	objective function
G_j	growth rate of face j (m s^{-1})
INF	agglomeration effect parameter
k_j	growth rate constant of face j (m s^{-1})
K_s	solubility product (mol l^{-1})^2
L	number mean size of a crystal population (m)
L_{agg}	number mean size of the agglomerates (m)
$L_{i,j}$	mean final size of the crystals studied for experiment i and face j (m)
L_{mon}	number mean size of the monocrystals (m)
n	number of particles
N	number of experiments
n_j	growth rate order of face j
P	perimeter (m)
S	surface of a particle (m^2)
s	standard deviation value
S_c	surface of the convex hull of the particle (m^2)
t_i	nucleation time of experiment i (s)
t_f	experiment end time (s)
u	normalized side length of a square
V_0	initial deionized water volume (l)
V_{Ca}	initial calcium chloride volume (l)
V_K	initial potassium oxalate volume (l)
x	side length of a square (m)
$\overline{x}$	average value
X_{agg}	number agglomerates fraction
X_{mon}	number monocrystals fraction

Greek letters

α	rejection criterion (%)
β	volume ratio
$\sigma=\frac{[Ox^{2-}][Ca^{2+}]}{K_s}-1$	supersaturation degree
ξ	simplicity morphological parameter
ω_1	number of erosions for the robustness compution
ω_2	number of erosions for the largest concavity index computation
Ω_1	robustness
Ω_2	largest concavity index

Superscripts and subscripts

s.f	single feed
d.f	double feed

References

[1] J. Garside, L. Brecevic, J. Mullin, The effect of temperature on the precipitation of calcium oxalate, J. Crystal Growth 57 (1982) 233–240.
[2] L. Brecevic, D. Kralj, J. Garside, Factors influencing the distribution of hydrates in calcium oxalate precipitation, J. Crystal Growth 970 (1989) 460–468.

[3] I. Houcine, E. Plasari, R. David, J. Villermaux, Influence of mixing characteristics on the quality and size of precipitated calcium oxalate in a pilot scale reactor, Trans. IChemE 75(A) (1997) 252–256.
[4] B. Marcant, R. David, Experimental evidence for and prediction of micromixing effects in precipitation, AIChE J. 37 (1991) 1698–1710.
[5] R. David, B. Marcant, Prediction of micromixing effects in precipitation: case of double-jet precipitators, AIChE J. 40 (1994) 424–432.
[6] A.S. Bramley, M.J. Hounslow, R.L. Ryall, Aggregation during precipitation from solution. Kinetics for calcium oxalate monohydrate, Chem. Eng. Sci. 52 (1997) 747–757.
[7] B. Tomazic, G.H. Nancollas, The kinetics of dissolution of calcium oxalates hydrates, J. Crystal Growth 46 (1979) 355–361.
[8] L. Lepage, R. Tawashi, Growth and characterization of calcium oxalate dihydrate crystals, J. Pharma. Sci. 71 (1982) 1059–1062.
[9] J.D. DeLong, D. Briedis, A technique for the study of growth rates of single crystals of sparingly soluble salts, J. Crystal Growth 71 (1985) 689–698.
[10] F. Grases, A. Millan, A. Garcia-Raso, Polyhydroxycarboxylic acids as inhibitors of calcium oxalate crystal growth: relation between inhibitory capacity and chemical structure, J. Crystal Growth 89 (1988) 496–500.
[11] M. Akbarich, R. Tawashi, Calcium oxalate crystal growth in the presence of mucin, Scanning Microsc. 5 (1991) 1019–1027.
[12] D. Skrtic, N. Filipovic-Vincekovic, V. Babic-Ivancic, The effect of dodecylammonium chloride on crystal growth of calcium oxalate, J. Crystal Growth 121 (1992) 197–201.
[13] E.J. Will, L.M.O. Bijvoet, L.J.M.J. Blomen, R. van der Linden, Growth kinetics of calcium oxalate monohydrate, J. Crystal Growth 64 (1983) 297–305.
[14] B. Bernard-Michel, S. Rohani, M.N. Pons, H. Vivier, H.S. Hundal, Classification of crystal shape using Fourier descriptors and mathematical morphology, Part. Part. Syst. Charact. 14 (1997) 193–200.
[15] H. Vivier, M.N. Pons, B. Bernard-Michel, T. Rolland, Quantification of particle morphology in powder process technology, Microsc. Microanal. Microstruct. 7 (1996) 467–475.
[16] H. Vivier, B. Marcant, M.N. Pons, Crystal shape analysis in precipitation and crystallization, in: Z.H. Rojkowski (Ed.), Proceedings of the 12th Symposium on Industrial Crystallization, vol. 2, Warsaw, 1993, pp. 53–58.
[17] H. Vivier, B. Marcant, M.N. Pons, Morphological shape characterization: application to oxalate crystals, Part. Part. Syst. Charact. 11 (1994) 150–155.
[18] M. Vucak, M.N. Pons, H. Vivier, Effect of operation conditions on the habit of oxalate crystals, Proceedings of the 13th Symposium on Industrial Crystallization, vol. 2, Toulouse, 1996, pp. 407–412.
[19] G.K. Pagenkopf, Introduction to Natural Water Chemistry, Marcel Dekker, New York, 1978.
[20] A. Packter, P. Chauhan, The precipitation of alkaline-earth metal and transition metal oxalates from aqueous solution. Induction periods and nucleation rates, Kristall und Technik 10 (1975) 621–631.
[21] J. Serra, Image Analysis and Mathematical Morphology, Academic Press, London, 1982.
[22] M.N. Pons, H. Vivier, J. Dodds, Particle shape characterization using morphological descriptors, Part. Part. Syst. Charact. 14 (1997) 272–277.
[23] M.N. Pons, H. Vivier, T. Rolland, Pseudo-3D shape description for facetted materials, Part. Part. Syst. Charact. 15 (1998) 100–107.
[24] H.M. Wodsworth, Handbook of Statistical Methods for Engineers and Scientists, McGraw-Hill, New York, 1990.
[25] B. Bernard-Michel, D. Jeanjean, M.N. Pons, H. Muhr, H. Vivier, J.L. Houzelot, Influence des paramètres opératoires sur la morphologie des cristaux, Récents Progrès en Génie des Procédés 11(54) (1997) 171–176.
[26] J.W. Einax, H.W. Zwanziger, S. Geiß, Chemometrics in Environmental Analysis, VCH, Munich, 1997.
[27] J. Zhang, E.B. Martin, A.J. Morris, Process monitoring using nonlinear statistical techniques, Chem. Eng. J. 67 (1997) 181–189.
[28] J.A. Dirksen, T.A. Ring, Fundamentals of crystallization: kinetic effects on particle size distributions and morphology, Chem. Eng. Sci. 46 (1991) 2389–2427.